Published in final edited form as:
Lab Invest. 2018 March ; 98(3): 380–390. doi:10.1038/labinvest.2017.132.

Microscale Characterisation of Prostate Biopsies Tissues using Optical Coherence Elastography and Second Harmonic Generation imaging

Yuting Ling[#1,2], **Chunhui Li**[#1,2], **Kanheng Zhou**[1,2], **Guangying Guan**[1,2], **Paul L. Appleton**[3], **Stephen Lang**[4], **David McGloin**[2], **Zhihong Huang**[1,2], and **Ghulam Nabi**[1]

[1]Division of Cancer Research, University of Dundee, Ninewells Hospital and Medical School, Dundee DD1 9SY, UK

[2]School of Science and Engineering, University of Dundee, Dundee DD1 4HN, UK

[3]Dundee Imaging Facility, University of Dundee, Ninewells Hospital and Medical School, Dundee DD1 9SY, UK

[4]Department of Pathology, University of Dundee, Ninewells Hospital and Medical School, Dundee DD1 9SY, UK

[#] These authors contributed equally to this work.

Abstract

Photonics, especially optical coherence elastography (OCE) and second harmonic generation (SHG) imaging are novel high-resolution imaging modalities for characterisation of biological tissues. Following our preliminary experience, we hypothesized that OCE and SHG imaging would delineate the microstructure of prostate tissue and aid in distinguishing cancer from the normal benign prostatic tissue. Furthermore, these approaches may assist in characterisation of the grade of cancer, as well. In this study, we confirmed a high diagnostic accuracy of OCE and SGH imaging in the detection and characterisation of prostate cancer for a large set of biopsy tissues obtained from men suspected to have prostate cancer using transrectal ultrasound (TRUS). The two techniques and methods described here are complementary, one depicts the stiffness of tissues and the other illustrates the orientation of collagen structure around the cancerous lesions. The results showed that stiffness of cancer tissue was approximately 57.63% higher than that of benign tissue (Young's modulus of 698.43 ± 125.29 kPa for cancerous tissue versus 443.07 ± 88.95 kPa for benign tissue with OCE. Using histology as a reference standard and 600kPa as a cut-off threshold, the data analysis showed sensitivity and specificity of 89.6% and 99.8% respectively. Corresponding positive and negative predictive values were 99.5% and 94.6% respectively. There was a significant difference noticed in terms of Young's modulus for different Gleason scores estimated by OCE (p value < 0.05). For SHG, distinct patterns of collagen distribution were seen for different Gleason grade disease with computed quantification employing a ratio of anisotropic to isotropic (A: I ratio) and this correlated with disease aggressiveness.

[**]**Correspondence**: GNabi@dundee.ac.uk, Tel: 0044 1382 660111.

Europe PMC Funders Author Manuscripts

Keywords

Prostate cancer; elasticity; mechanical biomarker; collagen; optical coherence elastography (OCE); second harmonic generation (SHG) microscopy

Introduction

Prostate cancer (PCa) is a heterogeneous disease with a multifocal origin1. The diagnosis is confirmed by histopathology of tissue samples obtained through TRUS guided biopsies. The disease is screened/suspected by a high serum prostate-specific antigen (PSA) levels and/or abnormal digital rectal examination (DRE). Cancer is characterised following histopathological verification under a microscope using the Gleason scoring system2 by a pathologist. The information obtained is utilized according to a risk- stratified approach and the treatment options are discussed with patients. However, the data obtained from the histopathological examination of the radical prostatectomy specimens indicates that a large disparity existed between the Gleason score of biopsy samples and the radical prostatectomy specimen. This incongruity has implications for patient counselling and therapy. In a meta-analysis of 14839 patients, Cohen et al.3 demonstrated that only 58% of patients' biopsy Gleason grade accurately predicted the final Gleason grade of radical prostatectomy. Similarly, Serefoglu et al.4 provided evidence that just 43.3% of patients had the same Gleason score for preoperative biopsy and postoperative radical prostatectomy specimens with the false-negative rate of more than 30%. Thus, the healthcare challenge is to improve accuracy of the Gleason grade characterisation of initial prostate biopsies as this would allow for more appropriate therapeutic choices.

Radical prostatectomy, a surgical option for localised disease seeking to cure, is primarily meant to remove all malignant tissues while preserving neurovascular bundles and continence mechanism for robust quality outcomes 5. Intraoperatively, the decision is based on a combination of preoperative imaging, biopsy histology and macroscopic assessment. The final decision on margin status, however, is confirmed after many days of surgery which is least helpful as corrective surgery is impossible in contrast to breast cancer6. Patients with positive surgical margins have a higher risk of cancer recurrence and necessitate further treatment. An intraoperative diagnostic technique that can reliably assess the margin status of tissues with regards to presence or absence of cancer cells would have a huge potential implication for surgical techniques and PCa patient outcomes. Frozen sectioning and imprint cytology are currently used but often unreliable7, 8. Optical imaging techniques have been explored to address this issue in a number of previous publications. A number of optical imaging techniques have been proposed, including optical coherence tomography (OCT)9 and Raman spectroscopy10, however the utility of tissue stiffness measurements has not been reported.

The stiffness difference perceived via DRE has been an effective technique for centuries to suspect PCa. Tissue from PCa has a higher elastic modulus than the normal prostate glandular tissue11. Changes in elasticity may indicate an abnormal pathologic process as the elasticity of tissue is a result of increased cell density and collagen deposition12, 13.

Measuring the elastic properties of prostate tissue has received increasing attention recently14–17. This can be deduced using ultrasound-based technology18. However, other imaging modalities such as magnetic resonance imaging (MRI) and OCT are also reported. Optical imaging with the advantage of a much higher microscale resolution has the potential to enhance the application limit of ultrasound and MRI19. Furthermore, this technology may uncover the microscopic heterogeneity of prostate tissue and even early tumours.

The working principle of OCT is similar to ultrasound, but it uses light instead of sound waves. OCT is a real-time, *in vivo* and non-invasive optical imaging technology with a high resolution and a fast acquisition speed. The use of OCT to perform elastography is a technique known as optical coherence elastography (OCE) with sub-nanometre displacement sensitivity 20. Although the penetration depth of OCE (1-2 mm) is much less than that of ultrasound and MRI, this limit can be overcome by developing fibre-optic like needle probes for elastography measurements21, 22. Our preliminary work utilising a novel quantitative OCE method clearly presented the promising results in *ex vivo* PCa detection with 120 biopsies from 10 patients17. We demonstrated that OCE can reliably differentiate between benign and malignant prostate tissues with a high diagnostic accuracy. The method also has potential for characterising different grades of PCa based on the change of tissue morphology and quantitative mechanical properties.

The preliminary study using OCE was limited to 10 patients, and the impact of Gleason score on stiffness needed further confirmation. Also, it is currently poorly understood whether the resulting elasticity images are faithful representations of the underlying micro-scale elastic properties. Extracellular matrix (ECM) remodelling23 is significant in cancer progression with collagen as the dominant structural component providing mechanical strength and flexibility to tissue. A technique that can identify and characterize features of the epithelial-stromal microenvironment is of great diagnostic potential and interest. An extension of our preliminary work was required along with peri-tumour collagen characterisation using SHG imaging.

SHG microscopy is a popular imaging tool for visualisation and characterisation of non-centrosymmetric 3D structures such as collagen in medicine and biology24. Fourier transform second harmonic generation (FT-SHG)25–27 was applied to quantify the changes in collagen morphology. The initial results28 indicated that the collagen in the prostate stroma had different patterns in normal and malignant biopsies depicted by SHG images, and the fibres of the malignant tissue tended to have a higher degree of preferred orientation than that which were normal as quantified by FT-SHG. The A:I ratio parameter based on the ratio between anisotropically and isotropically aligned collagen fibres, was applied to compute the regularity in collagen fibre orientation and correlate it with a variety of Gleason scores. Based on the initial results, we proceeded to test these results in a larger sample size.

We hypothesised that a combination of OCE and SGH imaging would narrow down the Gleason grade discrepancy between prostate biopsies and radical prostatectomy specimen. The study had the following objectives:

1. To estimate the diagnostic accuracy of OCE (2D and 3D) and SHG in the detection and grade characterisation of PCa in *ex vivo* prostate biopsies.

2. To determine the reliability of both these techniques in predicting the final radical prostatectomy Gleason grade of the disease from measurements of Young's modulus established through OCE and orientation of collagen according to SHG.

Patients and Imaging Methods

Selection of Cohort

This was a prospective study with institutional ethics approval (14/ES/0049) and informed consent from patients to report the research data. Seventy patients were recruited into the study, including 10 cases reported previously in our feasibility study. With a slight modification of the protocol from the feasibility study, we recruited 60 patients (age range 56-85) undergoing TRUS-guided biopsies for suspected PCa between April 2014 and December 2015. Thirty-seven men were confirmed to have PCa with a Gleason score ranging from 6 to 9. Amongst those without cancer, a number of histological findings were reported, such as benign prostatic hyperplasia (BPH), atypical small acinar proliferation (ASAP), and prostatitis and/or prostatic intraepithelial neoplasia (PIN).

We tested our hypothesis that *ex vivo* measurements of tissue stiffness on biopsy material may have an improved prediction of the final Gleason grade of radical prostatectomy in a small group of 11 patients undergoing laparoscopic radical prostatectomy employing a rapid prototyping mould- based approach published previously29.

Trans-rectal Ultrasound (TRUS) Guided Biopsies

All participants underwent the standard 12-core TRUS guided biopsies of prostate gland using an 18-G needle. The size of the biopsy samples ranged from approximately 0.8 mm to 1.2 mm in diameter and 5mm to 20 mm in length. Biopsies were immediately fixed using 10% neutral buffered formalin (50 mL) and stored in separate containers. The samples were allowed to be fully fixated over 24 hours according to the previous study protocol30. Measurement of stiffness point-wise along the length of biopsy specimen was conducted according to the OCE technique. The specimens were then analysed by an experienced uro-pathologist (SL) with a routine histological protocol via haematoxylin and eosin (H&E) staining. The uro-pathologist was unaware of stiffness data. The detailed pathological report included the presence/absence of malignancy, grade of cancer, percentage of cancer involvement in each core, and perineural infiltration.

The histopathological data of a total of 720 cores were categorised into non-cancerous prostate tissue (448 core biopsies) and cancerous prostate tissue (272 core biopsies), of which one patient was diagnosed with carcinosarcoma. The PCa tissue was further categorised into seven sub-groups based on different Gleason scores: 3+3, 3+4, 3+5, 4+3, 4+4, 4+5, and 5+4 in 58, 54, 4, 46, 48, 39, and 11 core biopsies, respectively. For estimation of collagen orientation around cancerous lesions using SHG microscopy, 42 biopsy samples were imaged (36 cancerous and 6 benign). The cancerous group was further divided into six sub-groups based on different Gleason scores: 3+3, 3+4, 4+3, 4+4, 4+5, and 5+4 with six core biopsies in each group.

Europe PMC Funders Author Manuscripts

Optical Coherence Elastography (OCE)

The system setup of OCT/OCE was based on our previous report 17 with slight modification. Briefly, the OCE consists of two main parts: vibration stimulation and displacement detection. An electromagnetic actuator was used for vibration stimulation, driven by a sine-wave modulated signal with the modulation frequency of ˜8 kHz. The maximum actuator displacement applied to the specimens was ˜1 μm to ensure the strain generated was in a pure linear-elastic regime. The vibrations could be transmitted from the actuator to compress the specimens and trigger vibration in the axial direction. Detection of the vibration signal was performed via a phase-sensitive optical coherence tomography (PhS-OCT) system. It employed a superluminescent diode (SLD) as the light source, with a central wavelength of ˜1302 nm and bandwidth of ˜85 nm, implemented by a spectral domain configuration. The sample arm had an objective lens of ˜18 mm focal length to deliver the detection light onto the specimens and coupled the vibration signals into the PhS-OCT for detection. The system had an axial resolution of ˜8.8 μm and a transverse resolution of ˜7.9 μm in air. The acquisition rate was determined by the spectrometer employed in the system which had a maximum rate of ˜76,000 A-scans/s. The dynamic range of the PhS-OCT system was measured to be ˜100 dB at 0.5-mm axial depth with a phase noise of 3 mrad. However, the SNR in the region of interest (ROI) of the tissue sample was ˜50 dB.

For the acquisition of a cross-sectional 2D structure and elastogram, the OCE probe beam stayed for 512 repeats during the A-line scan at every spatial location sequentially within the B-scan (a total of 256 locations) mode while the actuator repeatedly fired the stimulus. Thus, a complete B scan consists of 512 × 256 A-scans. The specimens were then scanned cross-sectionally from one end to the other at an interval of 50 μm. This ensured adequate details obtained to generate a 3D structure and elastogram of each biopsy. Further, the system had a minimized acquisition time that enabled that each pair of structure and elastogram were recorded from the same region of tissue. The acquisition time for a 3D OCE data set was 3 minutes for images with dimensions (xyz) of 3 mm × 2 mm × 2 mm.

After the acquisition of one data set, the transitional stage was moved 2.5 mm in the y direction for the next acquisition, and this was repeated until the whole biopsy core was scanned. During the OCE scanning, the biopsy core was placed on a 2% agar phantom with a thickness of approximately 8 mm which was an elasticity reference 31. The total scanning time for each biopsy was dependent on the biopsy length. The raw structure and elastogram data sets were processed by MATLAB R2015b (The MathWorks, Natick, MA, USA) for data processing 32 to generate structure and elastogram frames for each B-scan. The frames were then imported into Amira (Mercury Computer Systems, Berlin, Germany) and reconstructed into 3D data sets at full resolution.

Multiphoton SHG Microscopy

Images for the SGH technique were acquired with an upright multiphoton microscope TCS SP8 MP (Leica) at the Dundee Imaging Facility. The tunable near-IR laser (Spectra-Physics InSight DeepSee) produced linearly polarized pulses spectrally centred at 880 nm. After spatial filtering and collimation, the beam was sent to the galvo-scanner. Incident light at 880nm was focused onto the sample with a Leica HC PL Fluotar 10x 0.3NA objective.

Owing to momentum conservation, the SHG signal was especially directional and emitted mainly in the forward direction, being collected by a 0.9 NA condenser lens. The SHG signal was then filtered through a laser blocking filter (SP 680) and an SHG bandpass filter (440/20) and subsequently being detected with a standard photomultiplier. The SHG laser power was adjusted to around 50 mW so that sufficient signals were obtained without any obvious damage to the sample. The transmitted light image was obtained from a 488nm laser and collected in the forward transmitted light position via a 483/32 filter. A combination of z-stack and tile scan was utilized to acquire the whole area of the biopsy section automatically. Through identical settings, 12-bit images of 3352x3352 pixels were obtained using LAS X (Leica Application Suite X).

The alignment of collagen fibres in each section was quantified by Fourier transform second harmonic generation (FT-SHG) as described in the previous report 28. The processing algorithms were developed in Matlab R2015b (The MathWorks, Natick, MA, USA). This method was employed to identify the quantitative parameters that represent collagen orientation in the prostate biopsies through assessment of the spatial frequencies within an image using a 2D-FT. In a given plane, the direction the majority of fibres tend to align along is defined as the preferred orientation. Through 2D-FT, the high amplitudes on average oriented perpendicularly to the preferred orientation. To calculate the preferred orientation more rapidly, the original image was firstly divided into sub-images and categorized into three groups: negligible, anisotropic, or and isotropic. Negligible was defined if the SHG signal intensity in the area was low or nearly dark. The sub-images where collagen fibres had preferential orientation were labelled as anisotropic and the sub-images with many different directions were labelled as isotropic. Lastly, the overall orientation of the collagen fibres in each entire biopsy was quantified by applying the A:I ratio (the ratio of the number of anisotropic to isotropic sub-images).

Statistical Methods

A systematic statistical method was conducted by a statistician blinded to the OCE/SHG and histological data to investigate the reliability of quantitative OCE in differentiating benign and malignant prostate tissues as well as determining the sensitivity and specificity of this technique. Young's modulus (kPa) estimated from 720 biopsy cores by the OCE system was compared amongst malignant and benign tissues, as well as different Gleason scores. All the analyses were performed with SPSS v.22 (SPSS, Chicago, IL, USA). Differences between the groups were evaluated according to the Games-Howell test. A p value of 0.05 was considered to be statistically significant.

Results

2D Structural and Elastography of Prostate Biopsies

The images obtained from OCT and OCE imaging were directly compared with the images acquired after standard histopathological processing. The results suggested that micro-architecture on the order of 10 μm can be distinguished in prostatic tissue. Figure 1 presents the histological photo, OCT structural image, and OCE elastogram of various catalogues of prostate tissue. A clear biopsy-agar-air boundary can be seen in both the structural and

elasticity images. The signal strength of the elastogram decreased with the rise in imaging depth. This is because the accuracy of the phase measurement for the elastogram relies on the intensity level of the structural image, and the intensity of the vibration signals reduced at deeper locations.

The top of Figure 1 presents the images of histology, structure and elastogram of benign prostatic tissue. In the histological image Figure 1(1a) shows, an irregular boundary and/or hollow structure indicates the benign glandular lumens. However, there is no difference seen between the glandular lumens and the surrounding stromal tissue. For example, smooth muscle and fibroblastic stroma cannot be distinguished. Figure 1(1c) demonstrates in detail the elastic variance in various kinds of tissue in detail. The elasticity of the glandular lumens is higher than that of the stromal tissue. By comparing all elastograms and histological photos of benign prostate tissue, it is found that smooth muscle has the lowest stiffness at 378.4 kPa (SD = 48.9 kPa). The glandular lumens have higher stiffness at 530.6 kPa (SD = 30.9 kPa), whereas the stiffness of the fibroblastic stroma varies at 518.4 kPa (SD = 82.5 kPa).

Images of the histology, structure and elastogram of the PIN are illustrated in the middle of Figure 1. Subtle differences in tissue structure amongst benign, BPH, ASAP and PIN tissues can be elucidated in the structural images. The glandular lumens in Figure 1(2b) has a more irregular surface, which is confirmed by the histological phenotype in Figure 1(2a). The difference between PIN and benign prostate tissue is more evident in the elastogram Figure 1(2c). The PIN has higher stiffness than benign prostate biopsies, whereas BPH and ASAP have lower stiffness than benign prostate tissue. Notwithstanding, significant overlaps still existed amongst the elasticity range of the aforementioned kinds of prostate tissues.

A typical malignant glandular tissue with a Gleason score of 4+4 is found at the bottom of Figure 1. The lumens here serve as the main characteristic histologically to determine PCa aggressiveness. In Figure 1(3a), the malignant structures are significantly smaller than those in the benign glandular tissue and range in size from 10 μm to 50 μm. Therefore, OCT can identify microarchitecture of 10 μm or greater. Cancerous prostate tissue is observed to have a well-rounded shape without irregular gland lumens with higher light reflectivity. A significant increase of tissue stiffness is observed in Figures 1(3c). Therein, it is also noticed that the stiffer the prostate biopsy, the higher the Gleason sum, and the more aggressive the PCa.

3D Structural and Elastography of Prostate Biopsies

Figure 2 delineates 3D images of the structure and elastogram from benign and different grades of malignant PCa prostate biopsies. The en-face views of four different forms of data (structure, elastogram, overlay and histology) were obtained from five prostate cores of benign and different grades of malignant PCa with a Gleason sum 6 to 9. In Figure 2(b), an ascending trend of elasticity signal is observed in the region of malignant PCa with the concomitant increase in the Gleason sum. Additionally, the area of malignancy can be better portrayed by elastograms from OCE imaging than with a histological photograph. The bright areas in Figure 2(b) match the areas labelled by the red arrows in Figure 2(d) indicating the origin and end of the malignant area in the prostate biopsies.

Diagnostic Accuracy of OCE

In this study, three methods were utilized for statistical analysis in comparing different biopsy cores: 1) the average Young's modulus method, which is the weighted average Young's modulus value over the whole area associated with each biopsy, 2) the maximum Young's modulus which is the maximum Young's modulus value of all the B-scan elastograms across all biopsies, and 3) the threshold method which is the percentage of the data points comprising the Young's modulus values higher than 600 kPa amongst the data set for each biopsy.

The results from the statistical analysis of PCa and benign prostate tissue are illustrated and compared with the whisker plots in Figure 3. From these plots, a significant increase in stiffness can be observed (p value < 0.001) between the benign prostate tissue and PCa using any of the aforementioned three methods. In Figure 3(a), by comparing the elasticity data obtained from OCE and the corresponding histological report, PCa was suspected with Young's modulus higher than 600 kPa. Figures 3(b) and 3(c) demonstrate that a certain stiff area exists in the non-PCa biopsies, but most of it is below 30% which could suggest very low cancer involvement, but not recognizable.

The plot of the ROC analysis in Figure 4 is intended to evaluate the ability of quantitative OCE to diagnose PCa with the aforementioned three statistical analysis methods. Over 90% of the area is under the ROC curve. Amongst the three curves, the method of using average Young's modulus has the highest area under the curve (AUC; 93.9%) which supports OCE as a promising with a high capability for the diagnosis of PCa. The threshold method has an AUC of 93.6%, and the maximum method has the lowest AUC, albeit a still high accuracy (91.6%). Based on the threshold method for diagnostic accuracy, the biopsies with a Young's modulus higher than 600 kPa were treated as positive results for PCa, and the others were negative and can be considered cancer-free (benign) biopsies. Compared to the histological results, the data analysis showed that the sensitivity and specificity of the threshold method was 89.6% and 99.8% respectively. Moreover, the positive and negative predictive values calculated for this technique were 99.5% and 94.6% respectively.

The relationship between the Gleason score and the estimated Young's modulus is compared in Figure 5. The presence of the Gleason score in the histopathological results is of clinical significance when making an optimal decision for the individual patient. The average method stands out from the other methods. A significant difference was noticed amongst Young's modulus of different Gleason scores estimated by OCE (p value < 0.05) except for Gleason score 7 and 8 (p value = 0.765).

Collagen Orientation

According to the previous pilot study, a predominant reticular pattern of collagen fibres was seen in cancerous lesions in contrast to the more common papillary pattern of the benign part of tissues. However, the reticular pattern disappeared in highly-aggressive cancer such as Gleason 4+5. The A:I ratio was applied to compute the regularity in collagen fibre orientation and utilized to compare Gleason scores across prostate biopsies.. Generally, malignant cores were found to be more aligned than tose that were normal. . Moreover; the

A:I ratio increased with a higher Gleason score, which meaning that the collagen fibres tended to be more oriented as the prostate cancer became more aggressive.

It was noted and discussed in the previous study that a small fluctuation occurred with an advanced grade of cancer and that a Gleason score of 4+3 had a lower A:I ratio than a Gleason score of 3+4. The new study with an increased number of slides (42 in total) had similar findings. As shown in the Whisker plot in Figure 6(a), the orientation of the collagen fibres demonstrated a rising trend when the cancer was more aggressive, but it decreased for higher grade of malignancy, such as Gleason 8 and 9. Figure 6(b) illustrates that a Gleason 4+3 is less anisotropic than Gleason 3+4, which is consistent with what was observed in the previous study. Moreover, a Gleason score of 4+5 also had a higher tendency of alignment than a Gleason score of 5+4 in Figure 6(c). Therefore, a higher primary grade led to less oriented collagen fibres and a lower A:I ratio for a scenario of the same Gleason sum.

Collagen Orientation and Tissue Stiffness

Elastography can detect subtle elasticity differences across the biopsy with a high-resolution OCT system, and SHG imaging can illustrate collagen distribution and orientation with multiphoton microscopy. The correlation between OCE and SHG imaging is key to the understanding of the increased stiffness in malignant tissue. It was noted that the lower the Young's modulus, the less oriented the collagen fibres will be. As depicted in Figure 7, the biopsies with a Young's modulus lower than 800 kPa have a smaller A:I ratio.

Prediction of Histological Grade of Radical Prostatectomy

Eleven men underwent laparoscopic radical prostatectomy surgery, but two of them received a second biopsy before prostatectomy and were excluded from our study. Three patients (patients no.1, 3 and 7) had an upgrading in disease from a low to high Gleason score following radical prostatectomy (Table 1). Table 1 summarises biopsy stiffness, A:I ratio, initial Gleason grade, and final Gleason grade of radical prostatectomy. It is noteworthy that biopsy stiffness (kPa) is the weighted mean of the stiffest biopsy amongst 12 biopsies. The ROC curve of the analysis method using average Young's modulus has the highest AUC (93.9%). According to the analysis of variance (ANOVA) analysis of the average method, the upper bound for Gleason 6 is 626.41 kPa at a 95% confidence interval for mean. Hereby, these three patients should be stratified to a higher Gleason score.

Discussion

In this study, we demonstrated an optical characterization of the microstructural details of prostate tissue obtained from a large number of TRUS-guided biopsies using high-resolution optical coherence elastography (OCE) and second harmonic generation (SHG) imaging. The method appeared to be highly accurate in differentiating cancer from normal benign prostatic tissue. It also provided accurate characterisation of the Gleason grade based on the measurement of Young's modulus (tissue stiffness) and orientation of collagen around malignant lesions. OCT provides ultrastructural details of the tissues, and elastograms offer additional details and clarity. The technique could predict a higher Gleason grade disease with the final histopathological examination of a radical prostatectomy specimen. It may

help in bridging the disparity between histopathological Gleason grades of a TRUS biopsy and radical prostatectomy samples. Furthermore, the technique has real potential for being employed during surgery of the prostate to guide dissection between peripherally located cancer tissue and neurovascular bundles. With future engineering and research aimed at *in vivo* stiffness measurement and peri-tumoural collagen orientation, a multiscale imaging of PCa through a needle can be possible. The ultimate goals, to be achieved through future research following this work, are *in situ* detection and characterisation of PCa to permit a more precise focal treatment, and scanning of the surface of the excised prostate gland intraoperatively to provide the surgeon with an assessment of tumour margins within minutes of prostate removal. Several challenges must be addressed before a complete translational landscape is possible. Heterogeneity of tissues, including diathermied tissue on the surface of prostate, and presence of blood could have an effect on the penetration of light. However, an excised piece of tissue followed by washing with normal saline could be utilized within surgical theatres for margin status assessment.

As demonstrated in the structural images of prostate biopsies, clear differences were noticed between benign and malignant groups. Benign prostate biopsy tissues were observed to have irregular and hollow glandular lumens in 2D/3D images, whereas those that were malignant lacked a lumenal structure with an increment of light reflectivity. With further use of a different objective lens, the imaging resolution of OCT could be increased to 1-2 μm, which will uncover more structural details of a prostate biopsy, and enhance the capacity of optical biopsy. The functional OCE, used in this study measured vibrational amplitude (surrogate markers of mechanical properties) of the freshly obtained prostate specimens following mechanical loading of tissues. The tissue stiffness estimated from this parameter was then employed to categorise specimens into different histological classifications. Further quantitative 3D elastograms of a prostate biopsy were reconstructed in high resolution from consecutive 2D elastograms. Both structural images and elastograms obtained with the OCE system were compared with histopathology as a reference standard to evaluate the diagnostic accuracy of the technique. A high diagnostic accuracy (with AUC > 90%) of classification of normal and cancerous tissues was presented in an *ex vivo* setting according to quantitative OCE. Additionally, point-to-point comparison between histological imagery and elastograms illustrated a high accuracy when studying the underlying micro-scale elastic properties. This indicates that OCE can be a promising imaging tool for PCa detection with high sensitivity and specificity for malignant prostate diseases. With the average method, the stiffness of cancer biopsies was approximately 57.63% higher than that of those that were benign with corresponding stiffness values of 698.43 ± 125.29 kPa versus 443.07 ± 88.95 kPa.

The gold standard histopathological analysis requires the expertise of a trained histopathologist. An inter-observer variation exists between two histopathologists besides the difficulties in characterising lesions smaller than 3 mm. Microstructure, which may be missed by unaided eyes could explain the cases in this study where several areas of benign tissue had a higher stiffness than most. It was noted that the Young's modulus determined herein was higher than the literature15, 33. The prostate biopsy samples in this study were fixed in formalin before the OCE experiment, which ensured thesubsequent histopathological analysis of the cellular structure of the fixed biopsy was conducted

smoothly. Formalin is predominantly used to fix tissue by cross-linking the proteins and hindering the biological degradation process. It increases tissue stiffness which, to some extent, can bias the final elasticity of prostate biopsies. In our experiment, the timeline was precisely controlled to finish every experiment. As all samples were fully fixed30 in formalin for 24 hours, the extent of stiffness increase should have been the same for all the benign and malignant prostate tissues.

Within the tissue stroma, collagen is the main structural and mechanical component. Changes in collagen alignment have been reported in the stroma of breast cancer tissue when compared with normal breast tissue34, 35. In our study, the prostate biopsy was scanned via multiphoton microscopy with the SHG signal collected in the forward direction. The collagen pattern was then generated for each biopsy, and the orientation of collagen fibres was computed by FFT-SHG. The results from the SHG images were found to be correlated with the histological reports. The benign biopsy had a papillary collagen pattern whereas the malignant biopsy had a reticular collagen pattern. Isotropic collagen fibres were seen in the benign prostate tissue without a preferred orientation. However, the collagen distribution in the malignant biopsies tended to be more oriented to the same direction as the cancer became more aggressive. The correlation between collagen orientation and Gleason score, as well as the relationship between the orientation and tissue stiffness was analysed in this study. The collagen orientation details addressed the tissue stiffness increase in the malignant prostate compared with the benign version. In a small group of men undergoing radical prostatectomy, the Young's modulus and collagen orientation were used to predict the final Gleason histopathological score (Table 1). This certainly necessitates further work to assess any potential use of these techniques in risk stratifying men with PCa.

In conclusion, the imaging of the mechanical properties of prostate tissue using OCE and the orientation analysis of peri-tumoural collagen by SHG imaging presented the possibility of optical modalities for the identification and characterisation of PCa. The results from this study form the basis for future research employing these techniques for *in vivo* assessment of PCa and intraoperative assessment of tumour margins. The study is a first attempt at this scale to perform a detailed analysis of the microstructural details of human PCa tissue using elastograms and orientation of collagen around cancerous lesions. The biopsy stiffness and collagen orientation together constitute the new biomechanical markers of PCa with a very high diagnostic accuracy in terms of Gleason grade of cancerous tissues.

Acknowledgements

The authors want to express our gratitude to the patients and clinicians who have contributed to this study in Ninewells Hospital, Dundee DD1 9SY, UK. This work was supported by a Scottish Universities Physics Alliance (SUPA) PhD studentship and grants from Prostate Cancer UK (PCUK) and the Welcome Trust (Grant no. WT101468). We appreciate the histopathological assistance from Department of Pathology, University of Dundee, Ninewells Hospital and Medical School, Dundee DD1 9SY, UK. The authors also thank the Dundee Imaging Facility, School of Life Sciences, University of Dundee, Dundee DD1 4HN, UK and Tayside Tissue Bank, University of Dundee, Ninewells Hospital and Medical School, Dundee DD1 9SY, UK for the use of equipment, advice and support.

References

1. Arora R, Koch MO, Eble JN, et al. Heterogeneity of Gleason grade in multifocal adenocarcinoma of the prostate. Cancer. 2004; 100(11):2362–2366. [PubMed: 15160339]
2. Humphrey PA. Gleason grading and prognostic factors in carcinoma of the prostate. Modern Pathol. 2004; 17(3):292–306.
3. Cohen MS, Hanley RS, Kurteva T, et al. Comparing the Gleason prostate biopsy and Gleason prostatectomy grading system: the Lahey Clinic Medical Center experience and an international meta-analysis. European urology. 2008; 54(2):371–381. [PubMed: 18395322]
4. Serefoglu EC, Altinova S, Ugras NS, et al. How reliable is 12-core prostate biopsy procedure in the detection of prostate cancer? Canadian Urological Association journal = Journal de l'Association des urologues du Canada. 2013; 7(5–6):E293–298.
5. Chien GW, Slezak JM, Harrison TN, et al. Health-related quality of life outcomes from a contemporary prostate cancer registry in a large diverse population. BJU Int. 2017
6. Waljee JF, Hu ES, Newman LA, et al. Predictors of re-excision among women undergoing breast-conserving surgery for cancer. Ann Surg Oncol. 2008; 15(5):1297–1303. [PubMed: 18259820]
7. Cabioglu N, Hunt KK, Sahin AA, et al. Role for intraoperative margin assessment in patients undergoing breast-conserving surgery. Ann Surg Oncol. 2007; 14(4):1458–1471. [PubMed: 17260108]
8. Nunez LV, Buttaro MA, Morandi A, et al. Frozen sections of samples taken intraoperatively for diagnosis of infection in revision hip surgery. Acta Orthop. 2007; 78(2):226–230. [PubMed: 17464611]
9. Nguyen FT, Zysk AM, Chaney EJ, et al. Intraoperative Evaluation of Breast Tumor Margins with Optical Coherence Tomography. Cancer Res. 2009; 69(22):8790–8796. [PubMed: 19910294]
10. Haka AS, Volynskaya Z, Gardecki JA, et al. In vivo margin assessment during partial mastectomy breast surgery using Raman spectroscopy. Cancer Res. 2006; 66(6):3317–3322. [PubMed: 16540686]
11. Krouskop TA, Wheeler TM, Kallel F, et al. Elastic moduli of breast and prostate tissues under compression. Ultrasonic imaging. 1998; 20(4):260–274. [PubMed: 10197347]
12. Zaman MH, Trapani LM, Sieminski AL, et al. Migration of tumor cells in 3D matrices is governed by matrix stiffness along with cell-matrix adhesion and proteolysis. Proceedings of the National Academy of Sciences of the United States of America. 2006; 103(29):10889–10894. [PubMed: 16832052]
13. Tang J, Zhang Y, Zhang MB, et al. Tissue elasticity displayed by elastography and its correlation with the characteristics of collagen type I and type III in prostatic stroma. Asian journal of andrology. 2014; 16(2):305–308. [PubMed: 24435054]
14. Hoyt K, Castaneda B, Zhang M, et al. Tissue elasticity properties as biomarkers for prostate cancer. Cancer biomarkers : section A of Disease markers. 2008; 4(4–5):213–225.
15. Ahmad S, Cao R, Varghese T, et al. Transrectal quantitative shear wave elastography in the detection and characterisation of prostate cancer. Surg Endosc. 2013; 27(9):3280–3287. [PubMed: 23525883]
16. Woo S, Kim SY, Cho JY, et al. Shear Wave Elastography for Detection of Prostate Cancer: A Preliminary Study. Korean J Radiol. 2014; 15(3):346–355. [PubMed: 24843239]
17. Li C, Guan G, Ling Y, et al. Detection and characterisation of biopsy tissue using quantitative optical coherence elastography (OCE) in men with suspected prostate cancer. Cancer letters. 2015; 357(1):121–128. [PubMed: 25444932]
18. Varghese T. Quasi-Static Ultrasound Elastography. Ultrasound clinics. 2009; 4(3):323–338. [PubMed: 20798841]
19. Kennedy BF, Kennedy KM, Sampson DD. A Review of Optical Coherence Elastography: Fundamentals, Techniques and Prospects. Selected Topics in Quantum Electronics, IEEE Journal of. 2014; 20(2):272–288.
20. Kennedy KM, Ford C, Kennedy BF, et al. Analysis of mechanical contrast in optical coherence elastography. Journal of biomedical optics. 2013; 18(12):121508–121508. [PubMed: 24220762]

21. Kennedy KM, Kennedy BF, McLaughlin RA, et al. Needle optical coherence elastography for tissue boundary detection. Opt Lett. 2012; 37(12):2310–2312. [PubMed: 22739891]
22. Chau AH, Chan RC, Shishkov M, et al. Mechanical analysis of atherosclerotic plaques based on optical coherence tomography. Annals of biomedical engineering. 2004; 32(11):1494–1503. [PubMed: 15636110]
23. Tuxhorn JA, Ayala GE, Rowley DR. Reactive stroma in prostate cancer progression. J Urology. 2001; 166(6):2472–2483.
24. Campagnola P. Second harmonic generation imaging microscopy: applications to diseases diagnostics. Analytical chemistry. 2011; 83(9):3224–3231. [PubMed: 21446646]
25. Rao RAR, Mehta MR, Toussaint KC. Fourier transform-second-harmonic generation imaging of biological tissues. Optics express. 2009; 17(17):14534–14542. [PubMed: 19687932]
26. Matteini P, Ratto F, Rossi F, et al. Photothermally-induced disordered patterns of corneal collagen revealed by SHG imaging. Optics express. 2009; 17(6):4868–4878. [PubMed: 19293918]
27. Cicchi R, Kapsokalyvas D, Troiano M, et al. In vivo non-invasive monitoring of collagen remodelling by two-photon microscopy after micro-ablative fractional laser resurfacing. Journal of biophotonics. 2014; 7(11–12):914–925. [PubMed: 24339127]
28. Ling Y, Li C, Feng K, et al. Second harmonic generation (SHG) imaging of cancer heterogeneity in ultrasound guided biopsies of prostate in men suspected with prostate cancer. Journal of biophotonics. 2016 n/a-n/a.
29. Sheikh N, Wei C, Szewczyk-Bieda M, et al. Combined T2 and diffusion-weighted MR imaging with template prostate biopsies in men suspected with prostate cancer but negative transrectal ultrasound-guided biopsies. World J Urol. 2017; 35(2):213–220. [PubMed: 27236302]
30. Ling Y, Li C, Feng K, et al. Effects of fixation and preservation on tissue elastic properties measured by quantitative optical coherence elastography (OCE). Journal of Biomechanics. 2016
31. Li C, Guan G, Reif R, et al. Determining elastic properties of skin by measuring surface waves from an impulse mechanical stimulus using phase-sensitive optical coherence tomography. Journal of the Royal Society, Interface / the Royal Society. 2012; 9(70):831–841.
32. Guan G, Li C, Ling Y, et al. Quantitative evaluation of degenerated tendon model using combined optical coherence elastography and acoustic radiation force method. Journal of biomedical optics. 2013; 18(11):111417. [PubMed: 24193945]
33. Barr RG, Memo R, Schaub CR. Shear Wave Ultrasound Elastography of the Prostate Initial Results. Ultrasound Q. 2012; 28(1):13–20. [PubMed: 22357224]
34. Conklin MW, Eickhoff JC, Riching KM, et al. Aligned collagen is a prognostic signature for survival in human breast carcinoma. The American journal of pathology. 2011; 178(3):1221–1232. [PubMed: 21356373]
35. Provenzano P, Eliceiri K, Campbell J, et al. Collagen reorganization at the tumor-stromal interface facilitates local invasion. BMC Med. 2006; 4(1):1–15. [PubMed: 16412236]

Europe PMC Funders Author Manuscripts

Europe PMC Funders Author Manuscripts

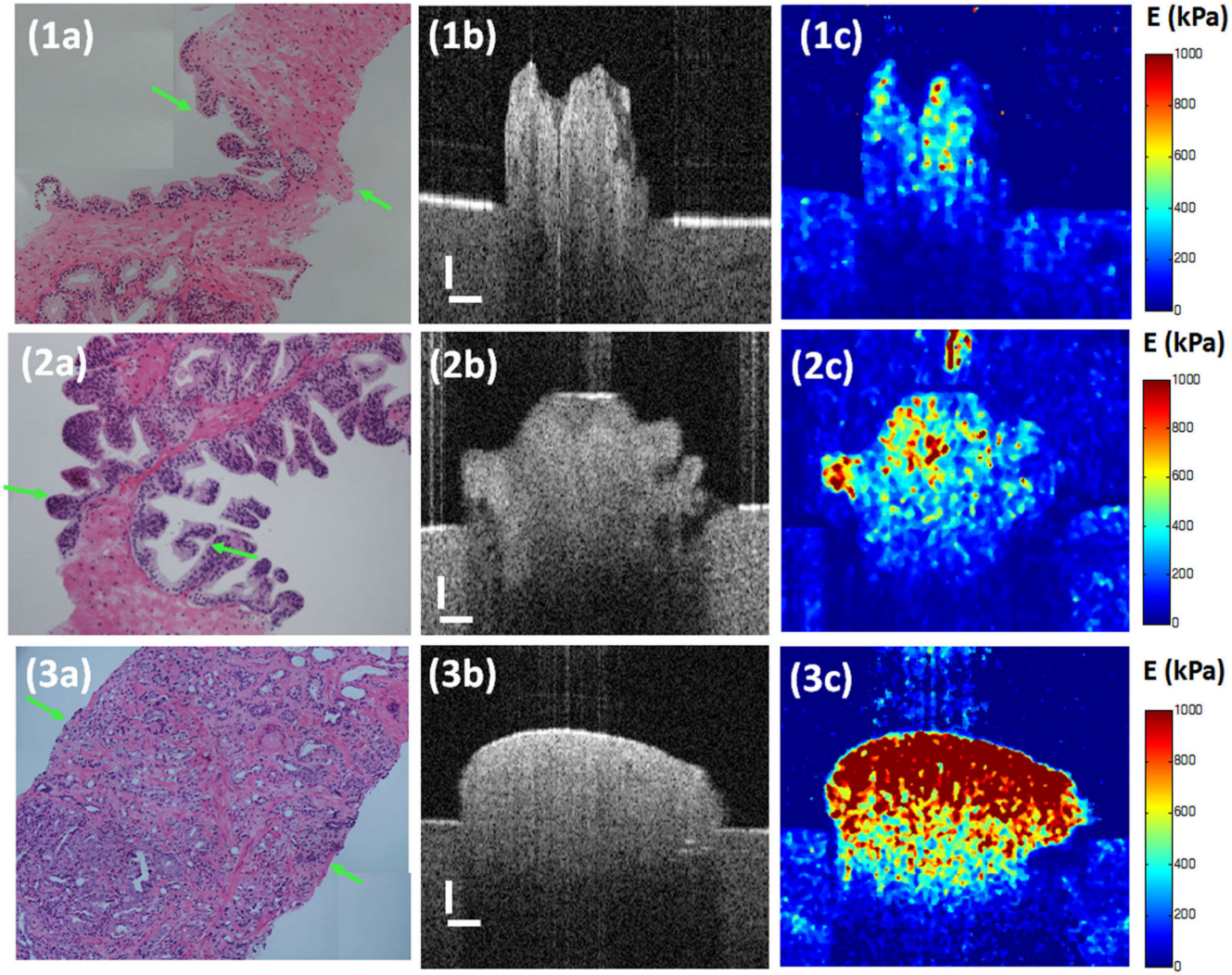

Figure 1.

Images of (a) histology, (b) cross sectional OCT structure and the corresponding (c) OCE elastogram of (1) benign prostate tissue, (2) prostatic intraepithelial neoplasia (PIN) and (3) malignant PCa with Gleason score 4+4. The scale is 200 μm. Young's modulus is in the unit of kPa

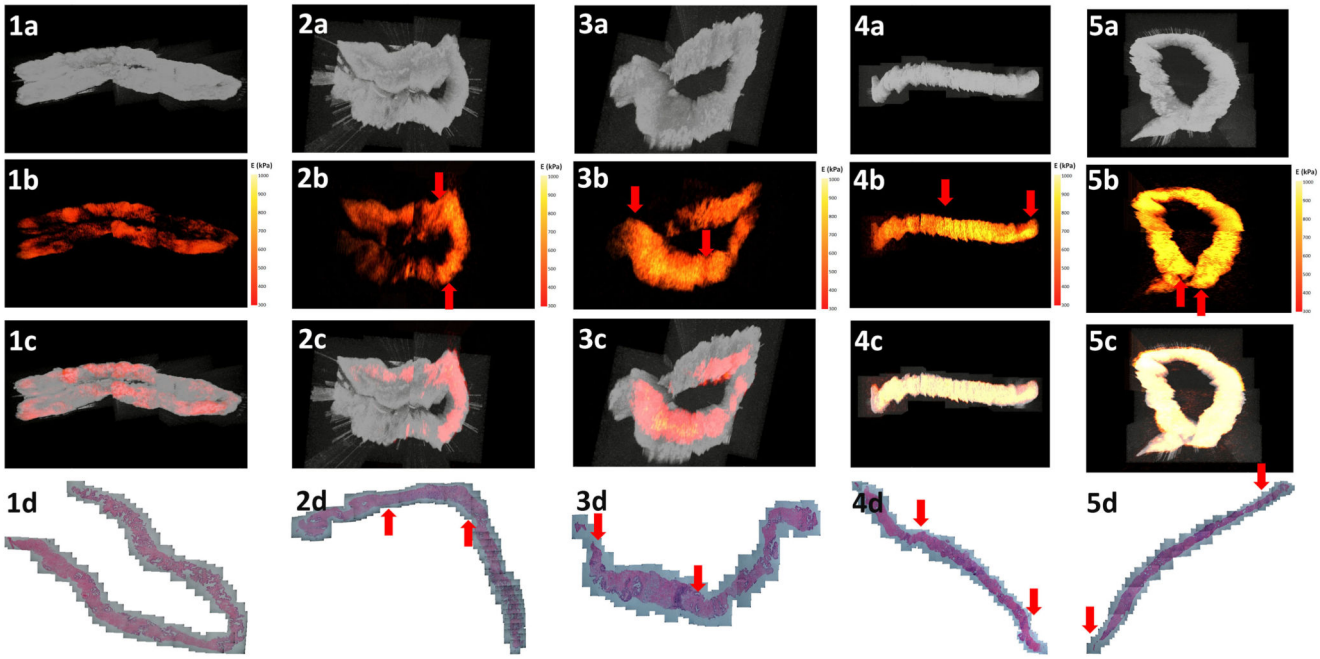

Figure 2.

3D visualization of (1) benign and PCa biopsies with Gleason score (2) 3+3 with cancer involvement 30%, (3) 3+4 with cancer involvement 40%, (4) 4+4 with cancer involvement 60% and (5) 4+5 with cancer involvement 80%. (a) OCT structural image, (b) OCE elastograms, (c) overlaid images from en face views and corresponding (d) histological photos. The red arrows in b and d indicate the origin and end of malignancy.

Europe PMC Funders Author Manuscripts

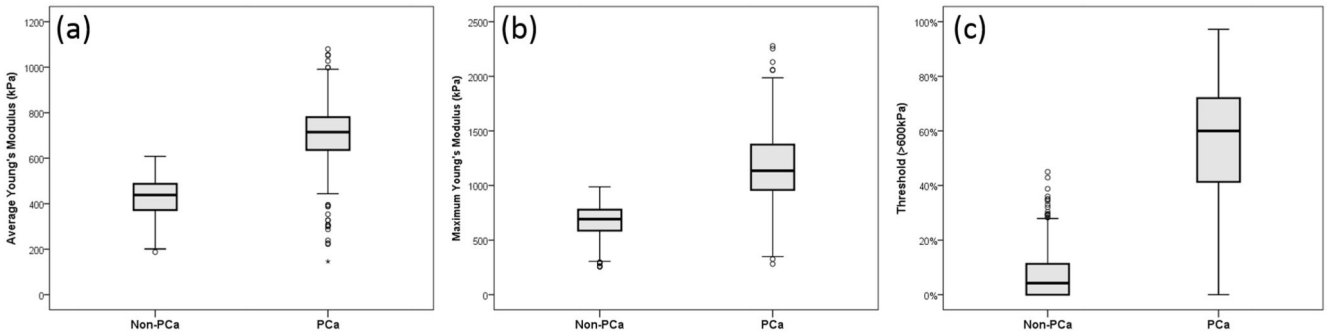

Figure 3.

Whisker plots of correlation of Young's modulus (kPa) and pathological outcomes using (a) average method, (b) maximum method and (c) threshold method.

Europe PMC Funders Author Manuscripts

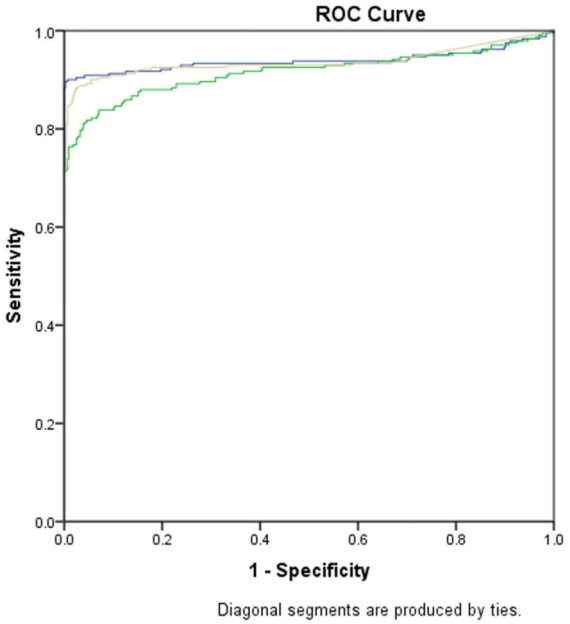

Area Under the Curve

Test Result Variable(s)	Area	Std. Error[a]	Asymptotic Sig.[b]	Asymptotic 95% Confidence Interval	
				Lower Bound	Upper Bound
Average	.939	.014	.000	.911	.966
Max	.916	.015	.000	.887	.944
Threshold	.936	.014	.000	.909	.963

The test result variable(s): Threshold has at least one tie between the positive actual state group and the negative actual state group. Statistics may be biased.

a. Under the nonparametric assumption

b. Null hypothesis: true area = 0.5

Figure 4.

ROC curves of PCa vs. benign using three statistical analysis methods.

Europe PMC Funders Author Manuscripts

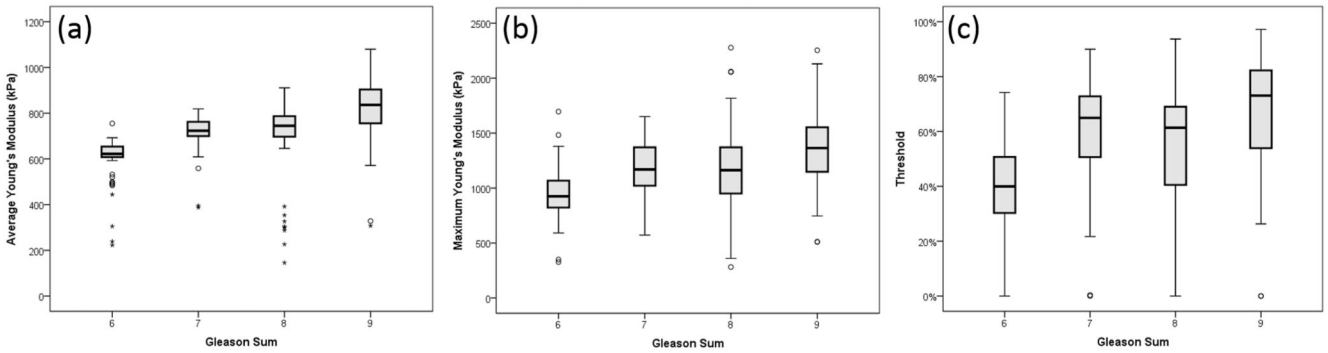

Figure 5.

Whisker plots of correlation of Gleason scores and Young's modulus (kPa) using (a) average method, (b) maximum method and (c) threshold method.

Europe PMC Funders Author Manuscripts

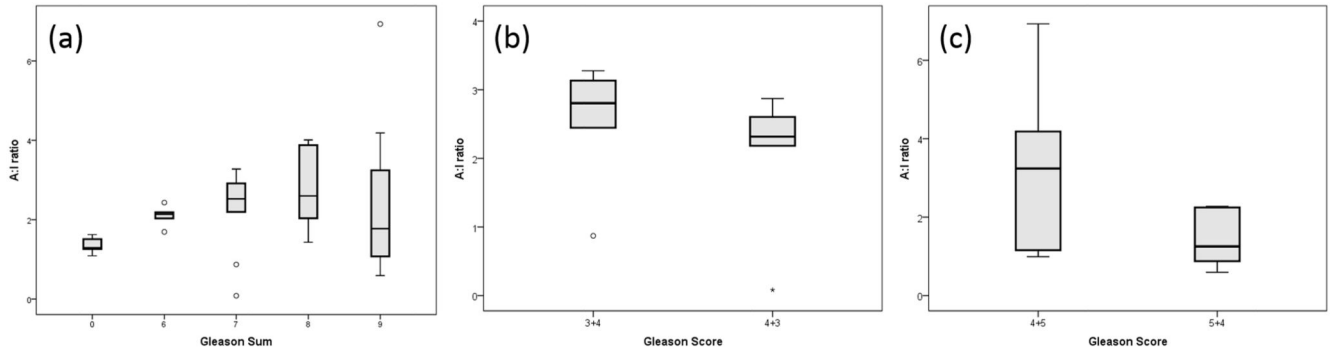

Figure 6.

Whisker plots of the relationship between collagen orientation (A.I ratio) and different Gleason scores. (a) Comparison among benign and malignant biopsies with different Gleason scores from 6 to 9, (b) comparison between Gleason 3+4 and 4+3, and (c) comparison between Gleason 4+5 and 5+4.

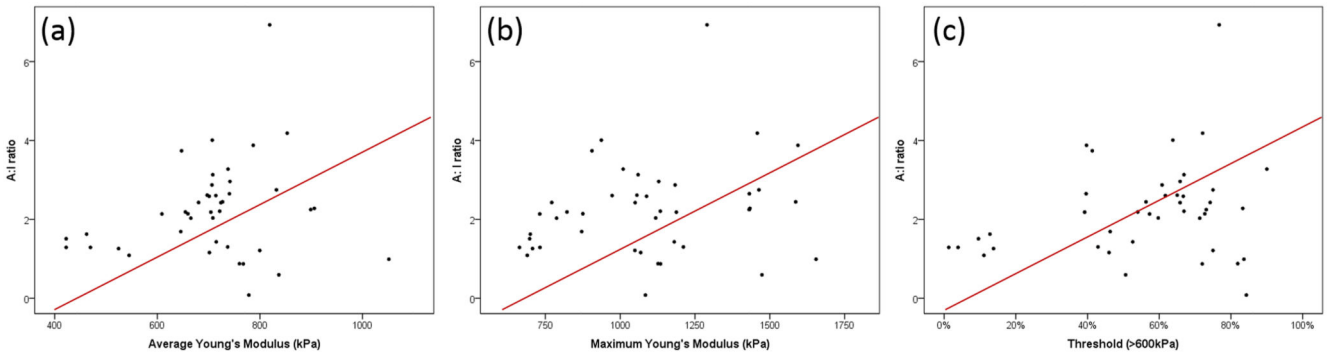

Figure 7.

Scatterplots of the correlation of Young's modulus and collagen orientation (A:I ratio) using the (a) average method, (b) maximum method and (c) threshold method.

Europe PMC Funders Author Manuscripts

Europe PMC Funders Author Manuscripts

Table 1

Disparity of Gleason score between initial TRUS biopsy and final prostatectomy.

Patient number	Biopsy stiffness (kPa)*	A:I ratio	Gleason grade of biopsies	Gleason grade of Radical prostatectomy	
1	631.07		3+3	3+4	7
2	795.16	1.79	3+3 3+4	3+4	7
3	649.02	1.29	3+3	3+4	7
4	809.61	2.55	4+3 4+4 4+5 5+4	4+5	9
5	707.69		3+3 3+4 4+3	3+4	7
6	900.99		3+5 4+4 4+5	4+5	9
7	658.93		3+3	3+4	7
8	728.25		3+3 3+4	3+4	7
9	739.24		3+3 4+3	4+3	7

* Biopsy stiffness (kPa) is the weighted mean of the stiffest biopsy amongst 12 biopsies.